IEICE TRANSACTIONS

on Communications

VOL. E105-B NO. 9
SEPTEMBER 2022

A PUBLICATION OF THE COMMUNICATIONS SOCIETY

The Institute of Electronics, Information and Communication Engineers
Kikai-Shinko-Kaikan Bldg., 5-8, Shibakoen 3chome, Minato-ku, TOKYO, 105-0011 JAPAN

PAPER

Asynchronous Periodic Interference Signals Cancellation in Frequency Domain

Satoshi DENNO[†a)], ***Senior Member and*** **Yafei HOU**[†], ***Member***

SUMMARY This paper proposes a novel interference cancellation technique that prevents radio receivers from degrading due to periodic interference signals caused by electromagnetic waves emitted from high power circuits. The proposed technique cancels periodic interference signals in the frequency domain, even if the periodic interference signals drift in the time domain. We propose a drift estimation based on a super resolution technique such as ESPRIT. Moreover, we propose a sequential drift estimation to enhance the drift estimation performance. The proposed technique employs a linear filter based on the minimum mean square error criterion with assistance of the estimated drifts for the interference cancellation. The performance of the proposed technique is confirmed by computer simulation. The proposed technique achieves a gain of more than 40 dB at the higher frequency part in the band. The proposed canceler achieves such superior performance, if the parameter sets are carefully selected. The proposed sequential drift estimation relaxes the parameter constraints, and enables the proposed cancellation to achieve the performance upper bound.

key words: *periodic interference, super resolution estimation, minimum mean square error (MMSE) estimation, frequency domain, asynchronous interference signals*

1. Introduction

High power transistors have been widely used in lots of vehicles such as electric cars. It is well-known that high power circuits with such high power transistors emit electromagnetic waves, while high power signals are traversed on the circuits. The electromagnetic waves affect other devices, for instance, receivers of wireless systems. Although low frequency signals are fed on the high power circuits, higher harmonics of the signals are enough to emit strong electromagnetic waves that interfere with wireless signals, because the power of wireless signals is small. To mitigate the performance degradation of wireless receivers due to the harmful undesired electromagnetic waves, many techniques have been proposed [1]. Shielding has been applied to prevent undesired electromagnetic waves from being radiated to such receivers [2]–[5]. To mitigate the emission of the undesired electromagnetic waves from the high power circuits, circuit layout has been investigated at the frequency band of interest [6]–[9]. Noise control techniques have been proposed for mitigating the peak power of the electromagnetic waves [10]. On the other hand, another approach to make wireless receivers robust against electromagnetic waves has also been sought. For instance, adaptive array antennas have been considered for the mitigation of undesired electromagnetic waves [11]–[13]. They need some additional hardware such as antennas. While they are very effective for alleviating the degradation due to the undesired electromagnetic waves, they cause some difficulties such as high cost, heavy weight, wide space and so on. Interference cancellation techniques have been proposed that need no additional hardware [14]–[16]. The frequency domain interference cancellation technique proposed in [14] can work well in digital wireless systems when the wireless signal is greater than interference signals. The frequency domain interference cancellation techniques in [15], [16] achieve superior interference mitigation performance despite of characteristics of wireless signals, even if numerous wireless signals are received. However, the cancelers need to synchronize with the interference signal. This means that the cancelers can remove only one undesired electromagnetic wave from the received signals.

This paper proposes a novel interference cancellation technique that achieves superior cancellation performance even if several interference signals are present. The proposed technique does not need to synchronize with any interference signal, assuming that the interference signals are periodic. When the interference signals are not synchronized with the proposed canceler, the interference signals are drifting at the canceler. The proposed canceler applies a super resolution technique to estimate the drift and removes the interference signals with the estimated drift.

This paper is organized as follows. Next section introduces a system model. The proposed canceler is explained in Sect. 3. The performance of the proposed technique is evaluated by computer simulation in Sect. 4 and Sect. 5 describes concluding remakes.

Throughout the paper, $\mathrm{E}[\alpha]$, $\Re[c]$, and $\Im[c]$ indicate the ensemble average of a variable α, a real part and an imaginary part of a complex number c. $\mathbf{A}^{\mathrm{T}}$, $\mathbf{A}^{\mathrm{H}}$, $(\mathbf{B})^{-1}$ and c^* represent transpose, Hermite transpose of a vector or a matrix $\mathbf{A}$, an inverse matrix of a matrix $\mathbf{B}$, and complex conjugate of a complex number c. $\mathrm{diag}[a_1 \cdots a_N]$ denotes a diagonal matrix with a_i in the diagonal positions where N indicates the size of the diagonal matrix. $\mathbf{I}_N$ and j denote the N-dimensional identity matrix and the imaginary unit.

2. System Model

We assume that a receiver with an antenna is put on a vehi-

Manuscript received November 15, 2021.
Manuscript revised February 10, 2022.
Manuscript publicized March 24, 2022.

[†]The authors are with Graduate School of Natural Science and Technology, Okayama University, Okayama-shi, 700-8530 Japan.
a) E-mail: denno@okayama-u.ac.jp

DOI: 10.1587/transcom.2021EBP3187

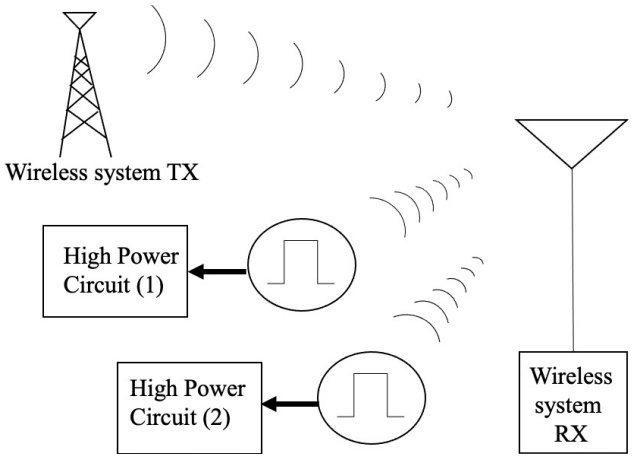

Fig. 1 System model.

cle for receiving wireless signals such as radio signals and television signals. Besides, high power circuits are installed on the vehicular to drive it. The high power circuits emit periodical undesired electromagnetic waves, which are also received at the antenna on the receiver. Let $y(t) \in \mathbb{C}$ denote the received signal where $t \in \mathbb{R}$ indicates a time index, the received signal is written as,

$$y(t) = \sum_{n=0}^{N_S-1} s_n(t) + \sum_{i=0}^{K-1} h_i x_i(t - \tau_i(t)) + n(t) \tag{1}$$

In (1), $s_n(t) \in \mathbb{C}$, $x_i(t) \in \mathbb{C}$, $h_i \in \mathbb{C}$, and $n(t) \in \mathbb{C}$ represent an nth wireless signal, an ith periodic interference signal caused by an undesired electromagnetic wave, a channel impulse response of the ith interference signal, and the additive white Gaussian noise (AWGN). In addition, $\tau_i(t) \in \mathbb{R}$, $N_s \in \mathbb{N}$, and $K \in \mathbb{N}$ denote delay time of the ith interference signal, the number of the wireless signals received at the antenna, and that of the interference signals, respectively. The system is illustrated in Fig. 1 where a wireless signal is received at an antenna of wireless system receiver as well as two undesired electromagnetic waves. The figure depicts the system model defined in (1) where the number of the wireless signals N_S and that of the periodic interference signals K are 1 and 2, respectively. The variable h_i denotes the channel impulse response between the antenna on the receiver and the interference signal generators shaped with the circles in the figure. We assume that most periodic interference signals are generated from regulators on vehicles, the cycles of the periodic interference signals are not so different from each other, but they are not synchronized with each other. The asynchronization among the interference signals prevents the receivers from being synchronized with those interference signals in principle.

3. Asynchronous Interference Cancellation

The received signals are sampled at the sampling rate $\frac{1}{T}$ where T denotes the cycle of the sampling. The sampled signals are converted to frequency domain signals by the discrete Fourier transform (DFT) as follows.

$$\begin{aligned} y_t(m) &= \sum_{n=0}^{N_F-1} y(t - nT)\, e^{j2\pi \frac{nm}{N_F}} \\ &= \sum_{i=0}^{N_S-1} s_{t,i}(m) + \sum_{i=0}^{K-1} h_i x_{t,i}(m) e^{j2\pi \frac{\tau_i(t)m}{N_F T}} + n_t(m) \end{aligned} \tag{2}$$

$N_F \in \mathbb{N}$ in (2) represents the number of the DFT points. $y_t(m) \in \mathbb{C}$, $s_{t,i}(m) \in \mathbb{C}$, and $s_{t,i}(m) \in \mathbb{C}$ denote mth frequency domain signals of the time domain signals $y(t)$, $s_i(t)$, and $n(t)$, the latter two variables of which are defined as, $s_{t,i}(m) = \sum_{n=0}^{N_F-1} s_i(t - nT) e^{j2\pi \frac{nm}{N_F}}$, and $n_t(m) = \sum_{n=0}^{N_F-1} n(t - nT) e^{j2\pi \frac{nm}{N_F}}$, respectively. In addition, $x_{t,i}(m)$ also represents mth frequency domain signal of the interference signal $x_i(t)$ defined as,

$$x_{t,i}(m) = \sum_{n=0}^{N_F-1} x_i(t - nT) e^{j2\pi \frac{nm}{N_F}}. \tag{3}$$

As is described above, the received signals are sampled and fed to the DFT implemented by the FFT (Fast Fourier Transform). It is natural to express time index t as a discrete time index. Because t is defined as the sampling timing of the first samples in the N_F samples that are provided to the DFT, the time index can be defined with integer multiples of $N_F T$, which is written as, $t = kN_F T + t_0$, where t_0 denotes an initial sampling offset. When the time index is expressed in the discrete format, the discrete received signal is defined as $y(k) \equiv y(kN_F T + t_0)$ where T and t_o are dropped from the notation in the left hand side of the equation. Hence, the discrete received signal is rewritten as follows.

$$y_k(m) = \sum_{n=0}^{N_S-1} s_{k,n}(m) + \sum_{i=0}^{K-1} h_i x_{k,i}(m) e^{j2\pi \frac{\tau_i(k)m}{N_F T}} + n_k(m) \tag{4}$$

As is described in the previous section, the interference signals $x_i(k)$ are not synchronized with each other. This means that every delay time $\tau_i(k)$ is drifting independently. To simplify the drifts, we approximate the drifting with a linear function, which is defined as $\tau_i(k) \equiv a_i kT + b_i$ where $a_i \in \mathbb{R}$ and $b_0 \in \mathbb{R}$ represents the drift during the sampling cycle T and an initial delay[†]. While the small drift does not degrade the DFT performance, the drift deteriorates the interference cancellation performance, which is explained below. To alleviate the performance deterioration, the drift is estimated in the following.

A received signal vector $\mathbf{Y}_k(m) \in \mathbb{C}^{N_d \times 1}$ is defined as $\mathbf{Y}_k(m) = \left(y_k(m)\ y_{k-N_p}(m) \cdots y_{k-(N_d-1)N_p}(m)\right)^T$ where N_d and N_p denote dimension of the vector $\mathbf{Y}_k(m)$ and spacing in time between the adjacent elements in the received signal vector. We introduce a correlation matrix $\mathbf{R}(m) \in \mathbb{C}^{N_d \times N_d}$ at

[†]If the drift a_i is small enough, the small drift does not affect the DFT conversion performance. Therefore, the small drift is neglected in the DFT defined in (2) and (4). The small drift means that the DFT cycle $N_F T$ is set close to integer multiples of the cycle of the interference signals.

the mth frequency, which is defined as follows.

$$\begin{aligned}\mathbf{R}(m) &= \frac{1}{N_{\mathrm{R}}}\sum_{k=(N_{\mathrm{d}}-1)N_{\mathrm{p}}}^{N_{\mathrm{R}}+(N_{\mathrm{d}}-1)N_{\mathrm{p}}-1}\mathbf{Y}_k(m)\,\mathbf{Y}_k(m)^{\mathrm{H}}\\ &\approx \sum_{n=0}^{N_{\mathrm{S}}-1}\sigma_{\mathrm{s},n}^2(m)\,\mathbf{I}_{N_{\mathrm{d}}}+\mathbf{R}_{\mathrm{x}}(m)+\sigma^2\mathbf{I}_{N_{\mathrm{d}}}. \end{aligned}\tag{5}$$

In (5), $N_{\mathrm{R}}\in\mathbb{N}$, $\sigma_{\mathrm{s},n}^2(m)\in\mathbb{R}$, $\sigma^2\in\mathbb{R}$, $\mathbf{I}_{N_{\mathrm{d}}}\in\mathbb{C}^{N_{\mathrm{d}}\times N_{\mathrm{d}}}$, and $\mathbf{R}_{\mathrm{x}}(m)\in\mathbb{C}^{N_{\mathrm{d}}\times N_{\mathrm{d}}}$ denote the number of the samples comprised of the correlation matrix, power of the nth wireless signal, that of the AWGN, the N_{d}-dimensional identity matrix, and the correlation matrix of the interference signals. Let an ith interference signal vector at the mth frequency point in the band $\mathbf{X}_{k,i}(m)\in\mathbb{C}^{N_{\mathrm{d}}\times 1}$ be defined as $\mathbf{X}_{k,i}(m)=\mathrm{e}^{\mathrm{j}2\pi\frac{b_i}{N_{\mathrm{F}}T}}\left(x_{k,i}(m)\mathrm{e}^{\mathrm{j}2\pi\frac{a_i km}{N_{\mathrm{F}}}}\cdots x_{k-(N_{\mathrm{d}}-1)N_{\mathrm{p}},i}(m)\mathrm{e}^{\mathrm{j}2\pi\frac{a_i(k-(N_{\mathrm{d}}-1)N_{\mathrm{p}})m}{N_{\mathrm{F}}}}\right)^{\mathrm{T}}$, the correlation matrix of the interference signals is defined as follows.

$$\mathbf{R}_{\mathrm{x}}(m)=\frac{1}{N_{\mathrm{R}}}\sum_{k=(N_{\mathrm{d}}-1)N_{\mathrm{p}}}^{N_{\mathrm{R}}+(N_{\mathrm{d}}-1)N_{\mathrm{p}}-1}\sum_{i_1,i_2=1}^{K}\mathbf{X}_{k,i_1}(m)\,\mathbf{X}_{k,i_2}(m)^{\mathrm{H}}\tag{6}$$

Since the correlation matrix of the interference signal is Hermitian as shown in the above, the correlation matrix can be decomposed as follows [17].

$$\begin{aligned}\mathbf{R}_{\mathrm{x}}(m) &= \mathbf{U}(m)\,\Gamma_{\mathrm{x}}(m)\,\mathbf{U}(m)^{\mathrm{H}}\\ &= \left(\bar{\mathbf{U}}(m)\ \ \tilde{\mathbf{U}}(m)\right)\begin{pmatrix}\bar{\Gamma}_{\mathrm{x}}(m) & \mathbf{0}\\ \mathbf{0} & \mathbf{0}\end{pmatrix}\begin{pmatrix}\bar{\mathbf{U}}(m)^{\mathrm{H}}\\ \tilde{\mathbf{U}}(m)^{\mathrm{H}}\end{pmatrix}\\ &= \bar{\mathbf{U}}(m)\,\bar{\Gamma}_{\mathrm{x}}(m)\,\bar{\mathbf{U}}(m)^{\mathrm{H}}\end{aligned}\tag{7}$$

In the above equation, $\mathbf{U}(m)\in\mathbb{C}^{N_{\mathrm{d}}\times N_{\mathrm{d}}}$ and $\Gamma_{\mathrm{x}}(m)\in\mathbb{C}^{N_{\mathrm{d}}\times N_{\mathrm{d}}}$ represent a unitary matrix and a diagonal matrix with eigenvalues in the diagonal positions. In addition, $\bar{\mathbf{U}}(m)\in\mathbb{C}^{N_{\mathrm{d}}\times K}$, $\tilde{\mathbf{U}}(m)\in\mathbb{C}^{N_{\mathrm{d}}\times(N_{\mathrm{d}}-K)}$, and $\bar{\Gamma}_{\mathrm{x}}(m)\in\mathbb{C}^{K\times K}$ denote orthogonal rectangular matrices, and a diagonal matrix with non-zero diagonal elements, which is defined as,

$$\bar{\Gamma}_{\mathrm{x}}(m)=\mathrm{diag}\left[\bar{\gamma}_1(m)\cdots\bar{\gamma}_K(m)\right],\tag{8}$$

where $\bar{\gamma}_i\in\mathbb{R}$ indicates ith eigenvalue of the matrix $\mathbf{R}_{\mathrm{x}}(m)$. Because we assume that the number of the interference signals K is much less than the vector length N_{d}, the diagonal matrix $\Gamma_{\mathrm{x}}(m)$ has zero diagonal elements. By substituting the correlation matrix in (7) for (5), the correlation matrix $\mathbf{R}(m)$ can be rewritten as follows.

$$\begin{aligned}\mathbf{R}(m) &= \mathbf{U}(m)\left\{\Gamma_{\mathrm{x}}(m)+\left(\sigma_{\mathrm{s}}^2(m)+\sigma^2\right)\mathbf{I}_{N_{\mathrm{d}}}\right\}\mathbf{U}(m)^{\mathrm{H}}\\ &= \mathbf{U}(m)\,\Gamma(m)\,\mathbf{U}(m)^{\mathrm{H}}\end{aligned}\tag{9}$$

In (9), $\Gamma(m)\in\mathbb{C}^{N_{\mathrm{d}}\times N_{\mathrm{d}}}$ and $\sigma_{\mathrm{s}}^2(m)\in\mathbb{R}$ represent a diagonal matrix and a total wireless signal power in the mth frequency, which are defined as $\Gamma(m)=\Gamma_{\mathrm{x}}(m)+\left(\sigma_{\mathrm{s}}^2(m)+\sigma^2\right)\mathbf{I}_{N_{\mathrm{d}}}$ and $\sigma_{\mathrm{s}}^2(m)=\sum_{n=0}^{N_{\mathrm{S}}-1}\sigma_{\mathrm{s},n}^2(m)$, respectively. Let the diagonal values of the matrix $\Gamma(m)$ be denoted as $\gamma_i(m)$, the diagonal matrix can be expressed as,

$$\begin{aligned}\Gamma(m) &= \mathrm{diag}\left[\gamma_1(m)\cdots\gamma_{N_{\mathrm{d}}}(m)\right]\\ &= \mathrm{diag}\Big[\bar{\gamma}_1(m)+\sigma_{\mathrm{s}}^2(m)+\sigma^2\cdots\bar{\gamma}_K(m)+\sigma_{\mathrm{s}}^2(m)+\sigma^2\\ &\quad\ \sigma_{\mathrm{s}}^2(m)+\sigma^2\cdots\sigma_{\mathrm{s}}^2(m)+\sigma^2\Big].\end{aligned}\tag{10}$$

Because all the values $\bar{\gamma}_1\cdots\bar{\gamma}_K$, and $\sigma_{\mathrm{s}}^2(m)+\sigma^2$ are positive, the eigenvalues have the following characteristics.

$$\gamma_1(m)>\cdots>\gamma_K(m)\gg\gamma_{K+1}(m)\simeq\cdots\gamma_{N_{\mathrm{d}}}(m)\tag{11}$$

If (7) is taken into account, the matrix $\mathbf{R}(m)$ can be rewritten by using the above relationship as,

$$\begin{aligned}\mathbf{R}(m) &= \bar{\mathbf{U}}(m)\begin{pmatrix}\gamma_1(m) & & \mathbf{0}\\ & \ddots & \\ \mathbf{0} & & \gamma_K(m)\end{pmatrix}\bar{\mathbf{U}}(m)^{\mathrm{H}}\\ &\quad+\tilde{\mathbf{U}}(m)\begin{pmatrix}\gamma_{K+1}(m) & & \mathbf{0}\\ & \ddots & \\ \mathbf{0} & & \gamma_{N_{\mathrm{d}}}(m)\end{pmatrix}\tilde{\mathbf{U}}(m)^{\mathrm{H}}.\end{aligned}\tag{12}$$

If we select the eigenvectors corresponding to the K biggest eigenvalues, i.e., $\gamma_1(m)\cdots\gamma_K(m)$, we can extract the orthogonal rectangular matrices $\bar{\mathbf{U}}(m)$ from the unitary matrix $\mathbf{U}(m)$. In a word, the rectangular orthogonal matrix $\bar{\mathbf{U}}(m)$ which contains the eigenvectors of the correlation matrix $\mathbf{R}_{\mathrm{x}}(m)$ can be extracted by means of the eigenvalue decomposition.

If the eigenvalues and the eigenvectors are obtained, we can estimate the correlation matrix of the interference signals $\mathbf{R}_{\mathrm{x}}(m)$. The correlation matrix of the interference signals $\mathbf{R}_{\mathrm{x}}(m)$ can be rewritten as follows (see Appendix).

$$\mathbf{R}_{\mathrm{x}}(m)\approx\sum_{i=0}^{K-1}\left|x_{k,i}(m)\right|^2\Psi_i(m)\tag{13}$$

$\Psi_i(m)\in\mathbb{C}^{N_{\mathrm{d}}\times N_{\mathrm{d}}}$ in (13) represents a Toeplitz matrix, which is defined as,

$$\begin{aligned}\Psi_i(m) &= \begin{pmatrix}1 & \cdots & \mathrm{e}^{\mathrm{j}2\pi\frac{a_i N_{\mathrm{p}}m(N_{\mathrm{d}}-1)}{N_{\mathrm{F}}}}\\ \vdots & \ddots & \vdots\\ \mathrm{e}^{-\mathrm{j}2\pi\frac{a_i N_{\mathrm{p}}m(N_{\mathrm{d}}-1)}{N_{\mathrm{F}}}} & \cdots & 1\end{pmatrix}\\ &= \mathbf{A}_i(m)\mathbf{A}_i(m)^{\mathrm{H}}.\end{aligned}\tag{14}$$

$\mathbf{A}_i(m)\in\mathbb{C}^{N_{\mathrm{d}}\times 1}$ denotes a steering vector defined in the following.

$$\mathbf{A}_i(m)=\begin{pmatrix}1\\ \mathrm{e}^{-\mathrm{j}2\pi\frac{a_i N_{\mathrm{p}}m}{N_{\mathrm{F}}}}\\ \vdots\\ \mathrm{e}^{-\mathrm{j}2\pi\frac{a_i N_{\mathrm{p}}m(N_{\mathrm{d}}-1)}{N_{\mathrm{F}}}}\end{pmatrix}\tag{15}$$

The correlation matrix $\mathbf{R}_{\mathrm{x}}(m)$ is rewritten with the steering vectors as,

$$\mathbf{R}_{\mathrm{x}}(m)\approx\mathbf{A}(m)\,\mathbf{D}(m)\,\mathbf{A}(m)^{\mathrm{H}}.\tag{16}$$

In (16), $\mathbf{A}(m) \in \mathbb{C}^{N_\mathrm{d} \times K}$ and $\mathbf{D}(m) \in \mathbb{C}^{K \times K}$ represent a steering matrix and a diagonal matrix defines as $\mathbf{A}(m) = (\mathbf{A}_1(m) \cdots \mathbf{A}_{N_\mathrm{d}}(m))$ and $\mathbf{D}(m) = \mathrm{diag}\left[\left|x_{k,1}(m)\right|^2 \cdots \left|x_{k,K}(m)\right|^2\right]$, respectively. The equation in (16) can be seen as factorization of the correlation matrix $\mathbf{R}_\mathrm{x}(m)$ with the steering matrix $\mathbf{A}(m)$ and the diagonal matrix $\bar{\Gamma}_\mathrm{x}(m)^\dagger$. The correlation $\mathbf{R}_\mathrm{x}(m)$ is also factorized in (9). If the two factorizations are compared, the following relationship can be found.

$$\mathbf{A}(m) = \bar{\mathbf{U}}(m)\mathbf{T}(m) \tag{17}$$

$\mathbf{T}(m) \in \mathbb{C}^{K \times K}$ represents a transform matrix.

We introduce two matrices defined as $\mathbf{J}_1 \in \mathbb{R}^{N_\mathrm{d} \times (N_\mathrm{d}-1)}$ and $\mathbf{J}_2 \in \mathbb{R}^{N_\mathrm{d} \times (N_\mathrm{d}-1)}$, which are defined as $\mathbf{J}_1 = (\mathbf{I}_{N_\mathrm{d}-1} \quad \mathbf{0}_{(N_\mathrm{d}-1)\times 1})^\mathrm{T}$ and $\mathbf{J}_2 = (\mathbf{0}_{(N_\mathrm{d}-1)\times 1} \quad \mathbf{I}_{N_\mathrm{d}-1})^\mathrm{T}$, respectively. If we see the characteristics of the matrix $\mathbf{A}(m)$ defined in (15), the following equation can be derived with the matrices $\mathbf{J}_1$ and $\mathbf{J}_2$ as follows.

$$\mathbf{J}_1\mathbf{A}(m) = \mathbf{J}_2\mathbf{A}(m)\Phi(m) \tag{18}$$

$\Phi(m) \in \mathbb{C}^{K \times K}$ denotes a diagonal matrix defined as $\Phi(m) = \mathrm{diag}(\phi_1(m) \cdots \phi_K(m))$, where $\phi_i(m) = \mathrm{e}^{-\mathrm{j}2\pi \frac{a_i N_\mathrm{p} m}{N_\mathrm{F}}}$. By substituting the matrix $\mathbf{A}(m)$ in (17) for (18), the above equation is rewritten as,

$$\mathbf{J}_1\bar{\mathbf{U}}(m)\mathbf{T}(m) = \mathbf{J}_2\bar{\mathbf{U}}(m)\mathbf{T}(m)\Phi(m). \tag{19}$$

If the matrix $\mathbf{T}(m)$ can be estimated with the matrix $\bar{\mathbf{U}}(m)$, we can estimate the diagonal matrix $\Phi(m)$. The matrices $\Phi(m)$ and $\mathbf{T}(m)$ to satisfy the above equation should be estimated simultaneously. This problem can be solved with super-resolution techniques such as the ESPRIT [18], [19]††. Those techniques give us an estimate of the diagonal matrix $\Phi(m)$. Let the estimate of the diagonal matrix be denoted by $\bar{\Phi}(m) \in \mathbb{C}^{K \times K}$ defined as $\bar{\Phi}(m) = \mathrm{diag}[\bar{\phi}_1(m) \cdots \bar{\phi}_K(m)]$ where $\bar{\phi}_p(m) \in \mathbb{C}$ indicates a pth estimate, an estimate of the drift $\bar{a}_i(m)$ can be obtained as follows.

$$\bar{a}_i(m) = \frac{N_\mathrm{F}}{2\pi m N_\mathrm{p}} \tan^{-1}\left(\frac{\Im\left[\bar{\phi}_i(m)\right]}{\Re\left[\bar{\phi}_i(m)\right]}\right) \tag{20}$$

In (20), $\tan^{-1}(\cdot)$ indicates the arctangent.

3.1 Sequential Drift Estimation

The output of the arctangent ranges from $-\frac{\pi}{2}$ to $\frac{\pi}{2}$ in principle. When the frequency index is high, i.e., m is large, the angular of the $\bar{\phi}_i(m)$, $2\pi\frac{a_i N_\mathrm{p} m}{N_\mathrm{F}}$, is easily made out of the range, even if the drift $a_i(m)$ is not big. To solve this problem, we propose a sequential drift estimation technique. When the frequency index m is low, the technique described in the previous section can exactly estimate the drift. The sequential drift estimation makes use of the nice performance at the lower frequency points in order to estimate the drifts at the higher frequencies. The proposed drift estimation technique estimates the drifts at the several frequency points. Let $\mathbf{B}$ denote a set of frequency indexes where the drift estimation is carried out, the set $\mathbf{B}$ is defined as $\mathbf{B} = \{m_1 ... m_{N_\mathrm{B}}\}$ where $m_l \in \mathbb{N}$ and $N_\mathrm{B} \in \mathbb{N}$ represent an lth entry and the number of entries in the set $\mathbf{B}$. Let $\hat{a}_i\left(m_{p-1}\right) \in \mathbb{R}$ indicate a drift estimated at the m_{p-1}th frequency point by the proposed sequential drift estimation, the proposed drift estimation technique estimate the drift $\hat{a}_i\left(m_p\right)$ at the m_pth frequency point as follows.

$$\begin{aligned}
\hat{\phi}_i^{(m_{p-1})}\left(m_p\right) &= \bar{\phi}_i\left(m_p\right)\mathrm{e}^{\mathrm{j}2\pi\frac{\hat{a}_i\left(m_{p-1}\right)m_p N_\mathrm{p}}{N_\mathrm{F}}} \\
\hat{a}_i\left(m_p\right) &= \frac{N_\mathrm{F}}{2\pi m_p N_\mathrm{p}} \tan^{-1}\left(\frac{\Im\left[\hat{\phi}_i^{(m_{p-1})}\left(m_p\right)\right]}{\Re\left[\hat{\phi}_i^{(m_{p-1})}\left(m_p\right)\right]}\right) - \hat{a}_i\left(m_{p-1}\right)
\end{aligned} \tag{21}$$

The sequential drift estimation estimates the drifts at the highest frequency point, i.e., the m_{N_B}th frequency point by iterating the signal processing defined in (21). The initial value $\hat{a}_i(m_1)$ is set to 0, i.e., $\hat{a}_i(m_1) = 0$.

If the correlation matrix is made from the infinite number of the vectors, i.e., $N_\mathrm{R} \to \infty$, the matrix $\mathbf{R}_\mathrm{x}(m)$ is exactly decomposed with the matrices $\mathbf{A}(m)$ and $\mathbf{D}(m)$. Actually, N_R is finite in real environment, which causes the correlation matrix $\mathbf{R}_\mathrm{x}$ to differ a little bit from the term in the right hand side of (16). This difference degrades the drift estimation performance, especially when the strong wireless signals are contained in the received signals.

3.2 Adaptive Cancellation

As is written in (4), the interference signals are weighted by not only $\mathrm{e}^{\mathrm{j}2\pi\frac{a_i k m + b_l}{N_\mathrm{F}}}$ but also a complex channel gain h_i. Since the drift a_i can be estimated by the proposed technique, the other part $h_i\mathrm{e}^{\mathrm{j}2\pi\frac{b_l}{N_\mathrm{F}}}$ is necessary to estimate exactly for successful interference cancellation. Because the part $h_i\mathrm{e}^{\mathrm{j}2\pi\frac{b_l}{N_\mathrm{F}}}$ is regarded as a time invariant term, the minimum mean square error (MMSE) is applied for the estimation of the time invariant terms in order to obtain the optimum cancellation performance in terms of the signal to noise power ratio (SNR). First of all, an error $e_k(m) \in \mathbb{C}$ is defined as,

$$\begin{aligned}
e_k(m) &= y_k(m) - \sum_{i=0}^{K-1}(w_i(m))^* \bar{x}_{k,i}(m)\,\mathrm{e}^{\mathrm{j}2\pi\frac{\bar{a}_i(m)mk}{N_\mathrm{F}}} \\
&= y_k(m) - \mathbf{W}(m)^\mathrm{H}\Theta_m(mk)\bar{\mathbf{X}}_k(m)
\end{aligned} \tag{22}$$

$\mathbf{W}(m) \in \mathbb{C}^{K \times 1}$ and $\Theta_m(mk) \in \mathbb{C}^{K \times K}$ denote an MMSE

†As is described below (A· 5), if the number of the vectors N_R becomes infinite, the eigenvalue decomposition in (16) will be carried out without any approximation, which leads the perfect drift estimation.

††The eigenvalue decomposition is applied to extract the interference signals from the correlation matrix. However, the eigenvalue decomposition conceals the steering vectors from the correlation matrix, even though the steering vectors are preserved in the correlation matrix through the eigenvalue decomposition. Super resolution techniques such as the ESPRIT can restore the steering vectors from the correlation matrix, which is going to be shown.

Table 1 Simulation parameters.

Interference signal	Rectangular pulse
DFT points N_{F}	128
Number of interference signals	2
Drift a_i	$1.0 \times 10^{-3}, 2 \times 10^{-3}$
Number of sample N_{R}	$2.0 \times 10^4 - N_{\mathrm{d}} N_{\mathrm{p}}$
Desired signals	Gaussian signal on every frequency index
Number of antennas	1
Channel model	AWGN

weight, and an estimated diagonal drift matrix, which are defined as $\mathbf{W}(m) = (w_1(m) \cdots w_K(m))^{\mathrm{T}}$ and $\Theta_m(mk) = \mathrm{diag}\left[\mathrm{e}^{\mathrm{j}2\pi \frac{\bar{a}_1(m)mk}{N_{\mathrm{F}}}} \cdots \mathrm{e}^{\mathrm{j}2\pi \frac{\bar{a}_K(m)mk}{N_{\mathrm{F}}}}\right]$ where $w_i(m) \in \mathbb{C}$ represents an ith weight. In addition, $\bar{\mathbf{X}}_k(m) \in \mathbb{C}^{K\times 1}$ represents a time invariant signal vector at the mth frequency point defined as $\bar{\mathbf{X}}_k(m) = (\bar{x}_{k,1}(m) \cdots \bar{x}_{k,K}(m))^{\mathrm{T}}$ where $\bar{x}_{k,i}(m) \in \mathbb{C}$ denotes a time invariant signal. The MMSE weight can be defined as follows.

$$\begin{aligned}\mathbf{W}(m) &= \arg\min_{\mathbf{W}} \sum_{k=1}^{N_{\mathrm{R}}} |e_k(m)|^2 \\ &= \left(\sum_{k=1}^{N_{\mathrm{R}}} \Theta_m(mk)\bar{\mathbf{X}}_k\bar{\mathbf{X}}_k^{\mathrm{H}}\Theta_m(mk)^{\mathrm{H}}\right)^{-1} \sum_{k=1}^{N_{\mathrm{R}}} \Theta_m(mk)\bar{\mathbf{X}}_k y_k^*(m)\end{aligned} \tag{23}$$

The proposed per-frequency cancellation technique comprises the FFT processing, the drift estimation and the adaptive cancellation. The sequential drift estimation needs m times complex multiplication as many as the per-frequency drift estimation. Since the drift estimation needs complicated computation such as the ESPRIT, the computational complexity is $\mathrm{O}(2N_{\mathrm{d}} - 2)^{3\dagger}$. In addition, the adaptive cancellation needs the weight matrix calculation with $N_{\mathrm{d}}\left(N_{\mathrm{d}}^2 + 1\right)$. However, they are needed only once at the beginning of the signal reception. On the other hand, the proposed adaptive cancellation has to perform the FFT and the linear filtering whenever the wireless signal is received. Hence, the complexity of the proposed technique is dominated by that of the linear filtering and the FFT. The complexity of the proposed technique is fairly small.

Though we assume that the interference signals are periodic in the time domain, we don't assume any other characteristics of the interference and the wireless signals. This means that the proposed technique mitigates the performance degradation due to periodic interference signals with any type of spectrum, despite of the characteristics of the wireless signals signals.

As is described in the introduction, no techniques have been proposed to cancel a few interference signals. Our proposed technique cancels severe periodic interference signals with small computational complexity, in spite of the wireless signals and spectrum of the interference signals. The performance is confirmed in the following section.

4. Simulation

The proposed technique is evaluated by computer simulations in an environment where two interference signals are received at the antenna as well as the wireless signals[††]. The wireless signals occupy all frequency points. In order to confirm that the proposed technique mitigates the performance degradation in any type of wireless systems, we evaluate the average performance of the proposed technique. According to the central limiting theory, the ensemble average of many signals is reduced to the Gaussian signal. This means that the average performance can be obtained by applying the Gaussian signal as a wireless signal. Therefore, the Gaussian signal is used as a wireless signal. Even though the proposed technique can handle with any type of periodic signals, we apply periodical rectangular pulse with duty cycle of 50% as the interference signal, because regulators generate such rectangular pulses that cause the undesired electromagnetic wave. The drift of the interference signals are set to 1.0×10^{-3} and 2.0×10^{-3} except in Fig. 8. We apply the ESPRIT with the TLS algorithm. Only one antenna is put on the receiver. Since the undesired electromagnetic waves are propagated to the antenna in a vehicle, the propagation channel is regarded static. This paper applies the AWGN channel as a representative of static channels, because this is a first step of our challenge[†††]. The time invariant signal vector $\bar{\mathbf{X}}_k(m)$ is set to $\bar{\mathbf{X}}_k(m) = (1 \quad 1)^{\mathrm{T}}$. The proposed drift estimation applies a set $\mathbf{B}$ with 4 entries, i.e., $N_{\mathrm{B}} = 4$. The set $\mathbf{B} = \{8, 48, 88, 128\}$ is used for the drift estimation. Hence, $N_{N_{\mathrm{B}}} = N_4 = 128$[††††].

4.1 Drift Estimation Performance

Figure 2 shows the drift estimation performance of the proposed technique with respect to the frequency index m. The vector length N_{d} is 20, i.e., the correlation matrix size is 20×20, and the spacing N_{p} is 100. The carrier power to interference power ratio (CIR) is -10 dB, and 10 dB. The interference power to the AWGN power ratio (INR) is changed from 15 dB to 35 dB. The estimation performance is getting better as the frequency index is higher. The drift

[†]We assume that that the ESPRIT with the total least squares (TLS) algorithm is applied [20].

[††]Because this is our first step of our challenge, the performance is evaluated by computer simulation. The theoretical performance analysis is one of our important future works.

[†††]While the proposed technique can be used in fading channels, the performance could depend on channel realization. Adaptive cancellation in fading channels and the performance evaluation will be included in our future works.

[††††]We have selected the set $\mathbf{B}$ where the highest element is N_{F} and the adjacent elements are equally spaced for the sequential drift estimation achieving its potential performance. The number of the elements N_{B} is selected for the lower complexity implementation, while the sequential drift estimation would achieve better performance as the number of the elements increases. There is a tradeoff between the complexity and the performance. Optimization of the number of the set $\mathbf{B}$ is one of our future works.

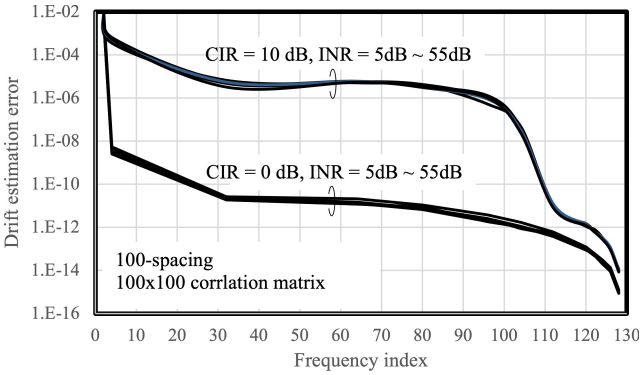

Fig. 2 Drift estimation performance at frequency points.

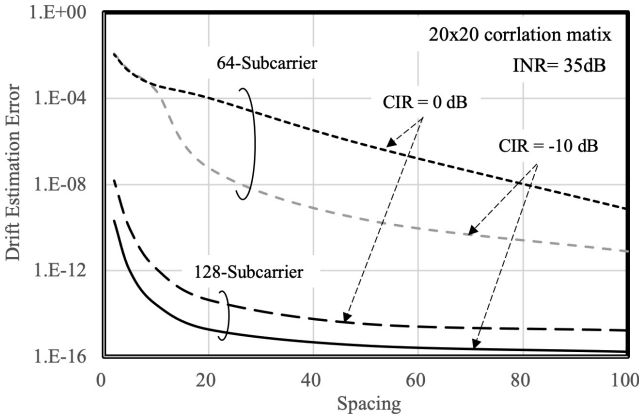

Fig. 3 Drift estimation performance v.s. spacing.

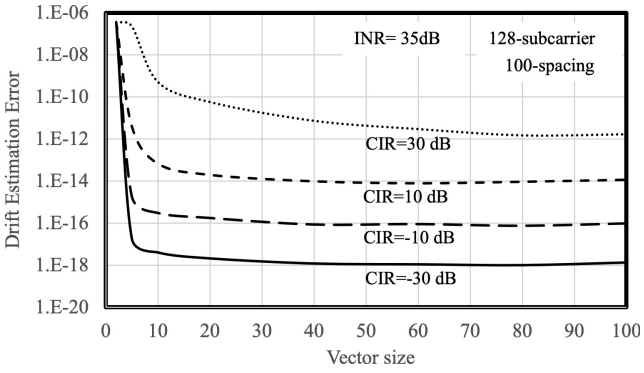

Fig. 4 Drift estimation performance vs vector size.

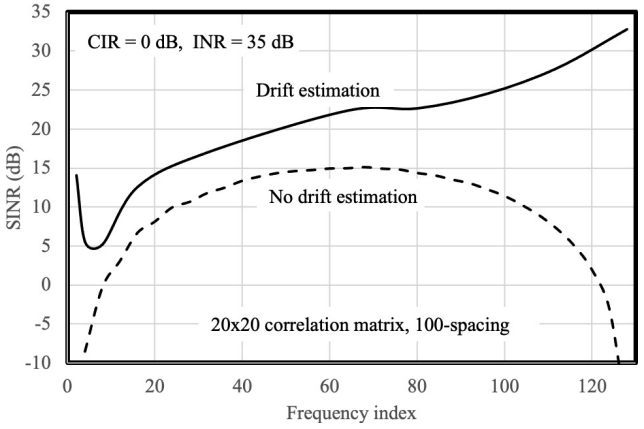

Fig. 5 Drift estimation performance at frequency points.

estimation error is defined as $\frac{1}{K}\sum_{l=1}^{K}\mathrm{E}\left[|a_l(m)-\bar{a}_l(m)|^2\right]$ in the figure. The estimation performance is improved as the CIR is reduced. Since the rectangular pulse with duty cycle of 50 % is used, the CIR of the received frequency domain signals is getting larger toward the center in the frequency points. This is the reason why the estimation performance at the higher edge is better in the frequency points. However, the estimation performance becomes worse as the frequency index gets smaller. As is shown in the vector $\mathbf{X}_{k,i}(m)$, the rotation angle due to the drift becomes smaller as the frequency index m gets small. In other words, when the frequency index m is small, the phase rotation term $\mathrm{e}^{\mathrm{j}2\pi\frac{a_i N_\mathrm{p} m}{N_\mathrm{F}}}$ becomes small. Because the small term is easily collapsed by the AWGN, the estimation performance is getting degraded as the frequency index m becomes smaller.

Figire 3 shows the drift estimation performance with respect to the spacing N_p. The correlation matrix size is 20×20, and the INR is 35 dB. The CIR is set to 0 dB and -10 dB. The estimation performances at the 64th and the 128th frequency points are compared. While the performance is dependent on the frequency index, the estimation performance is improved as the spacing gets longer. On the other hand, as is shown in Fig. 2, the higher frequency index enables the proposed technique to achieve better estimation performance. We apply the frequency index of 128 for the estimation. Since the estimation performance is only gradually improved as the spacing gets longer, we hereafter uses $N_\mathrm{p} = 100$ in this paper.

Figure 4 shows the drift estimation performance at the frequency index of 128 with respect to the vector size N_d, i.e., the correlation matrix size $N_\mathrm{d} \times N_\mathrm{d}$. The INR is 35 dB. The CIR is changed from -30 dB to 30 dB. The spacing N_p is set to 100. The estimation error is improved as the CIR gets smaller. As long as the CIR is less than 10 dB, the proposed technique achieves similar estimation performance if the vector size is bigger than 20. The vector with $N_\mathrm{d} = 20$ is hereafter used for the performance evaluation.

4.2 Cancellation Performance

The proposed cancellation technique is evaluated in terms of the signal power to the noise and interference power ratio (SINR). Figure 5 shows the cancellation performance of the proposed cancellation technique with respect to the frequency index. The vector size N_d and the spacing N_p are 20 and 100, respectively. The CIR and the INR are set to 0 dB and 35 dB, respectively. The cancellation performance without drift estimation is added as a reference. Because the rectangular pulse with duty cycle of 50% is applied, the CIR of the input signals at both the edges is the worst in all the frequency points. When the drift estimation is not applied to the adaptive cancellation, the CIR at the

frequency index gets worse as the frequency index comes closer to the both edges. This means that the interference cancellation without drift estimation is not able to improve the CIR at the both edge of the frequency band points. On the other hand, the proposed canceler improves the SINR performance. Although the drift estimation performance degrades as the frequency index decreases as shown in Fig. 2, such estimated rough drift helps the canceller to improve the SINR performance at the lower edge of the frequency band. As the frequency index increases, such estimated rough drift causes the severe cancellation performance degradation, because the phase in the phase rotation term becomes greater. However, as the frequency index becomes more than 6, the estimated drift gets very exact, which improves the SINR performance. The performance gain is maximized at the higher edge, i.e., $m = 128$, because the proposed technique achieves the best drift estimation performance at the highest edge. The proposed technique attains a gain of more than 40 dB at the edge. Because the cancellation is truly necessary at the edge, the performance of the proposed technique is mainly evaluated at the frequency index of 128.

Figure 6 shows the cancellation performance at the frequency index of 128 with respect to the spacing N_{p}. In the figure, the proposed technique with the sequential drift estimation is added. To contrast with the sequential drift estimation, the original drift estimation defined in (20) is named as "per-frequency drift estimation" in the figure. The 20×20-correlation matrix is used and the vector length N_{d} is 20. The proposed technique with the per-frequency drift estimation achieves the performance upper bound when the spacing is set between 50 and 120[†]. As the spacing is smaller than 50, the SINR is more degrading. On the other hand, the proposed technique with the sequential drift estimation achieves the performance upper bound, as long as the spacing N_{p} is more than 80. However, the performance is degraded when the spacing N_{p} is less than 80. The proposed technique with the sequential drift estimation achieves the upper bound with wider spacing range than that with the per-frequency drift estimation.

Figure 7 shows the cancellation performance at each frequency index where the spacing N_{p} is lengthened to 500. The CIR is set to -10 dB and the INR is 15 dB and 35 dB. The 20×20-correlation matrix is applied. The proposed technique with the per-frequency drift estimation carries out the drift estimation defined in (20), and applies the estimated drifts for the adaptive cancellation at every frequency index. On the other hand, the proposed technique with the sequential drift estimation estimates the drifts at the frequency index of $m_{N_{\mathrm{B}}}$, i.e., 128, and applies the estimated drifts for the adaptive cancellation at all the frequency points. While the proposed technique with the per-frequency drift estimation achieves the performance upper bound at the frequency points of lower than 30, the performance is degraded as the frequency index gets more than 30. On the other hand, the proposed technique with the sequential drift estimation achieves the performance upper bound at all the frequency points.

Figure 8 shows the cancellation performance at the frequency index of 128 with respect to the drift in terms of the SINR. The horizontal axis is the drift of one interference

[†]When the CIR is -10 dB, the signal power is 10 dB smaller than that of the interference power. If the INR are 35 dB, the noise power is 35 dB smaller than the interference power. This means that the carrier power to noise power ratio (CNR) is 25 dB. On the other hand, when the CIR and the INR are equal to 0 dB and 35 dB, the CNR is 35 dB.

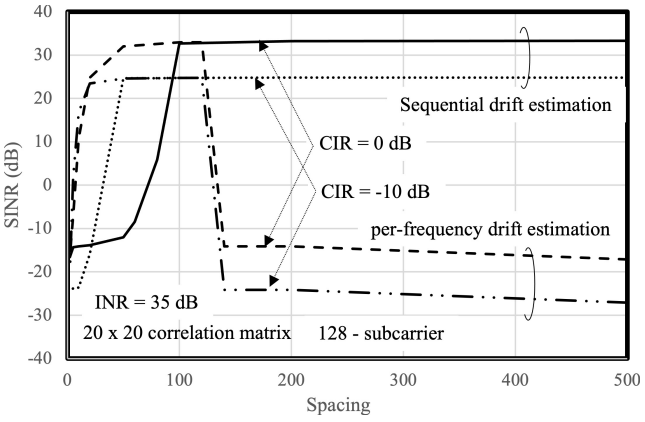

Fig. 6 SINR performance at frequency points.

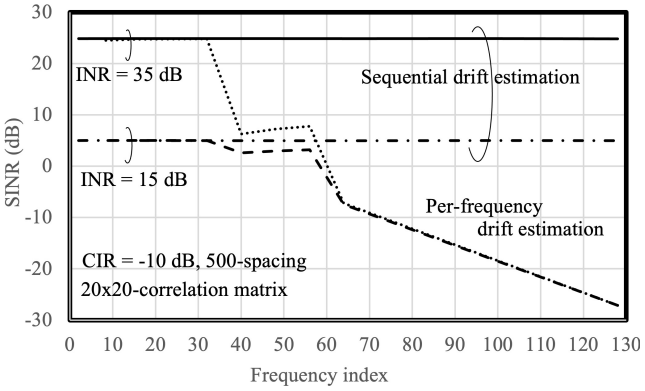

Fig. 7 SINR performance comparison.

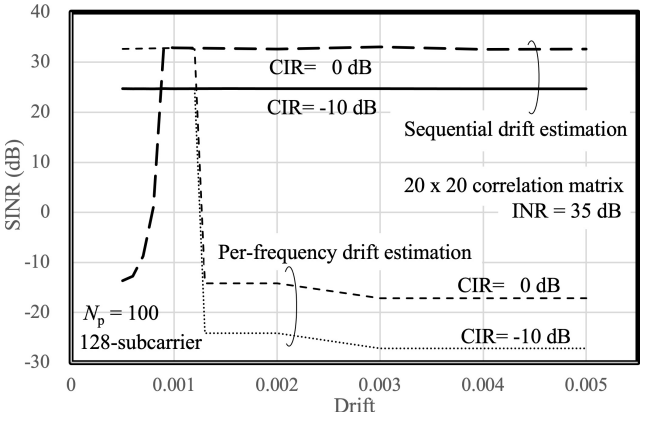

Fig. 8 SINR v.s. drift.

signal, and the drift of the second interference signal is two times as much as the horizontal axis. The spacing N_p and the vector length N_d are set to 100 and 20, respectively. The INR is 35 dB, and the CIR is set to −10 dB and 0 dB. When the proposed technique with the per-frequency drift estimation is used, the cancellation performance is easily deteriorated if the drift is bigger than 1.2×10^{-3} in spite of the CIR. On the other hand, the proposed technique with the sequential drift estimation achieves the performance upper bound in spite of the drift, when the CIR is equal to −10dB. When the CIR is 0dB, the performance upper bound is achieved as long as the drift is more than 1.0×10^{-3}. If the drift is less than 1.0×10^{-3}, the cancellation performance is suddenly degraded, because the drift estimation performance is degraded as inferred in Fig. 2. Because we can not exactly know how much the interference signals are drifted, the sequential drift estimation can be regarded as a useful technique to keep the superior performance even if the drift is deviated more.

5. Conclusion

This paper has proposed a novel interference cancellation technique that makes radio receivers robust against undesired electromagnetic waves emitted from high power circuits such as those on electric vehicles. The proposed interference cancellation technique removes the interference signals caused by the undesired electromagnetic waves from the received signals, even if several interference signals are present in the received signals. The proposed interference cancellation technique achieves superior interference cancellation performance, assuming that the interference signals are periodic in the time domain, even if the interference signals are not synchronized with each other. The proposed technique calculates a correlation matrix in the frequency domain, and applies super resolution techniques such as the ESPRIT to estimate the drifts of the interference signals. The proposed technique cancels the interference signals based on the linear filtering called "adaptive cancellation" with the estimated drifts. The minimum mean square estimation is applied to the adaptive canceler. Moreover, this paper proposes a sequential drift estimation for the proposed technique to keep the performance at all the frequency points.

The performance of the proposed technique is confirmed by computer simulation. The proposed technique achieves superior drift estimation performance, especially, at higher frequency points. The proposed technique attains a gain of more than 40 dB at the higher frequency points. The proposed canceler achieves the upper bound of the interference cancellation performance with the estimated drift, however, if the parameter sets are carefully selected. The sequential drift estimation relaxes the parameter selection. The proposed technique with the sequential drift estimation achieves the the performance upper upper bound even if the drift is more that 4.0×10^{-2}.

6. Acknowledgments

This work was supported by JSPS KAKENHI Grant Number JP21K04061.

References

[1] A.R. Ruddl and R. Armstrong, "Review of current EMC standards in relation to vehicles with electric powertrains," the 2013 International Symposium on Electromagnetic Compatibility, pp.298–303, Brugge Belgium, Sept. 2013.
[2] E.F. Vance, "Shielding effectiveness of braided-wireshields," IEEE Trans. Electromagn. Compat., vol.EMC-17, no.2, pp.71–77, May 1975.
[3] F. Briault, M. Hélier, D. Lecointe, J.C. Bolomey, and R. Chotard, "Broad-band modeling of a realistic power converter shield for electric vehicle applications," IEEE Trans. Electromagn. Comapat., vol.42, no.4, pp.477–486, 2000.
[4] K.-C. Kim, C.S. Jin, and J. Lee, "Magnetic shield design between interior permanent magnet synchronous motor and sensor for hybrid electric vehicle," IEEE Trans. Magn., vol.45, no.6, pp.2835–2838, 2009.
[5] M. Xu, Y. Wang, X. Li, X. Dong, H. Zhang, H. Zhao, and X. Shi, "Analysis of the influence of the structural parameters of aircraft braided-shield cable on shielding effectiveness," IEEE Trans. Electromagn. Compat., vol.62, no.4, pp.1028–1036, 2020.
[6] M. Pahlevaninezhad, D. Hamza, and P.K. Jain, "An improved layout strategy for common-mode EMI suppression applicable to high-frequency planar transformers in high-power DC/DC converters used for electric vehicles," IEEE Trans. Power Electron., vol.29, no.3, pp.1211–1228, 2014.
[7] T. Matsusima, T. Watanabe, Y. Toyota, R. Koga, and O. Wada, "Increase of common-mode radiation due to guard trace voltage and determination of effective via-location," IEICE Trans. Commun, vol.E92-B, no.6. pp.1929–1936, June 2009.
[8] A. Zadehgol, and A.C. Cangellaris, "Isotropic spatial filters for suppression of spurious noise waves in sub-gridded FDTD simulation," IEEE Trans. Antennas Propag., vol.59, no.9, pp.3272–3279, Sept. 2011.
[9] C.-H. Huang and T.L. Wu, "Analytical design of via lattice for ground planes noise suppression and application on embedded planar EBG structures," IEEE Trans. Compon. Packag. Manuf. Technol., vol.3, no.1, pp.21–30, Jan. 2013.
[10] N. Mutoh, M. Nakanishi, M. Kanesaki, and J. Nakashima, "EMI noise control methods suitable for electric vehicle drive systems," IEEE Trans. Electromagn. Comapat., vol.47, no.4, pp.930–937, 2005.
[11] M. Fujimoto, T. Tabata, T. Hori, and T. Hori, "Effect of constraint vector on adaptive array based on PI algorithm," IEICE Trans. Commun. (Japanese edition), vol.J97-B, no.2, pp.208–215, Feb. 2014.
[12] S. Ito, M. Fujimoto, T. Hori, M. Takanashi, and I. Shinya, "Periodic noise suppression system using frequency shift," IEICE Trans. Commun. (Japanese edition), vol.J98-B, no.7, pp.681–688, July 2015.
[13] S. Ito, M. Fujimoto, T. Hori, T. Harada, and Y. Hattori, "Noise suppresion system for AM radio using hilbert transform," IEICE Communications Express, vol.5, no.5, pp.142–146, May. 2016.
[14] J. Armstrong and H.A. Suraweera, "Impulse noise mitigation for OFDM using decision directed noise estimation," 8th IEEE Intern. Symposium Spread Spectrum Techniques and Applications, pp.174–178, Sydney Australia, 2004.
[15] Y. Sato, S. Denno, and T. Karube, "Adaptive periodic interference cancellation for narrow-band wireless systems," IEICE Trans. Commun. (Japanese edition) vol.J101-B, no.8, pp.627–636, Aug. 2018.
[16] Y. Kimura, S. Denno, and Y. Hou, "Adaptive sideband selection for pefiodic interference cancellation," IEICE Trans. Commun.

(Japanese edition), vol.J102-B, no.8, pp.595–604, Aug. 2019.
[17] R.A. Horn and C.R. Johnson,, Matrix Analysis, Cambridge University Press, 1985.
[18] R. Roy, A. Paulraj, and T. Kailath, "ESPRIT-A subspace rotation approach to estimation of parameters of cisoids in noise," IEEE Trans. Acoust., Speech, Signal Process., vol.ASSP-34, no.5, pp.1340–1342, 1986.
[19] M. Haadt and J.A. Nossek, "Unitary ESPRIT: How to obtain increased estimation accuracy with a reduced computational burden," IEEE Trans. Signal Process., vol.45, no.5, pp.1232–1242, 1995.
[20] B. Ottersten, M. Viberg, and T. Kailath, "Performance analysis of the total least squares ESPRIT algorithm," IEEE Trans. Signal Process., vol.39, no.5, pp.1122–1135, 1991.
[21] W.C. Jakes, Microwave Mobile Communications, IEEE Press, 1994.

Appendix: Correlation Matrix

When N_{R} is large enough, the correlation matrix can be approximated with its ensemble average as,

$$\mathbf{R}_{\mathrm{x}}(m) \approx \frac{1}{N_{\mathrm{R}}}\mathrm{E}\left[\sum_{k=(N_{\mathrm{d}}-1)N_{\mathrm{p}}}^{N_{\mathrm{R}}+(N_{\mathrm{d}}-1)N_{\mathrm{p}}-1}\sum_{i_1=1,i_2=1}^{K}\mathbf{X}_{k,i_1}(m)\,\mathbf{X}_{k,i_2}(m)^{\mathrm{H}}\right]. \tag{A·1}$$

Let $r_m(p,q)$ denote the (p,q) element of the matrix $\mathbf{R}_{\mathrm{x}}(m)$, because the interference signals and the drift are independent each other, the element $r_m(p,q)$ can be written as,

$$\begin{aligned} r_m(p,q) &= \frac{1}{N_{\mathrm{R}}} \\ &\quad \bullet\mathrm{E}\left[\sum_{k=(N_{\mathrm{d}}-1)N_{\mathrm{p}}}^{N_{\mathrm{R}}+(N_{\mathrm{d}}-1)N_{\mathrm{p}}-1}\sum_{i_1,i_2=1}^{K}x_{k-(p-1)N_{\mathrm{p}},i_1}(m)x_{k-(q-1)N_{\mathrm{p}},i_2}(m)^{*}\right. \\ &\quad \left.\mathrm{e}^{\mathrm{j}2\pi\frac{\left\{\left(a_{i_1}-a_{i_2}\right)k-\left(a_{i_1}(p-1)-a_{i_2}(q-1)\right)N_{\mathrm{p}}\right\}m}{N_{\mathrm{F}}}}\right]\mathrm{e}^{\mathrm{j}2\pi\frac{b_{i_1}-b_{i_2}}{N_{\mathrm{F}}T}} \\ &= \frac{1}{N_{\mathrm{R}}}\sum_{k=(N_{\mathrm{d}}-1)N_{\mathrm{p}}}^{N_{\mathrm{R}}+(N_{\mathrm{d}}-1)N_{\mathrm{p}}-1}\sum_{i_1,i_2=1}^{K}\mathrm{E}\left[x_{k-(p-1)N_{\mathrm{p}},i_1}(m)x_{k-(q-1)N_{\mathrm{p}},i_2}(m)^{*}\right] \\ &\quad \bullet\mathrm{E}\left[\mathrm{e}^{\mathrm{j}2\pi\frac{\left\{\left(a_{i_1}-a_{i_2}\right)k-\left(a_{i_1}(p-1)-a_{i_2}(q-1)\right)N_{\mathrm{p}}\right\}m}{N_{\mathrm{F}}}}\right]\mathrm{e}^{\mathrm{j}2\pi\frac{b_{i_1}-b_{i_2}}{N_{\mathrm{F}}T}} \end{aligned} \tag{A·2}$$

Because we assume that $a_{i_1} \neq a_{i_2}$ if $i_1 \neq i_2$, the terms with $\mathrm{E}\left[\mathrm{e}^{\mathrm{j}2\pi\frac{\left(a_{i_1}-a_{i_2}\right)km}{N_{\mathrm{F}}}}\right]$ $i_1 \neq i_2$ disappear. The element $r_m(p,q)$ is again rewritten as,

$$\begin{aligned} r_m(p,q) &= \frac{1}{N_{\mathrm{R}}}\sum_{i=1}^{K}\mathrm{e}^{-\mathrm{j}2\pi\frac{a_i(p-q)N_{\mathrm{p}}m}{N_{\mathrm{F}}}} \\ &\quad \bullet\sum_{k=(N_{\mathrm{d}}-1)N_{\mathrm{p}}}^{N_{\mathrm{R}}+(N_{\mathrm{d}}-1)N_{\mathrm{p}}-1}\mathrm{E}\left[x_{k-(p-1)N_{\mathrm{p}},i}(m)x_{k-(q-1)N_{\mathrm{p}},i}(m)^{*}\right] \end{aligned} \tag{A·3}$$

Since the drift a_i expresses the deviation of the interference signals $x_i(t)$ in the time domain, a part of its frequency domain signal, $x_{t,i}(m)$ is not time selective. $x_p(m)$ does not depend on time index p, i.e., $x_{p,i}(m) = x_{q,i}(m)$ even if $p \neq q$.

This reduces the above equation to the following equation.

$$r_m(p,q) = \sum_{i=1}^{K}\mathrm{e}^{-\mathrm{j}2\pi\frac{a_i(p-q)N_{\mathrm{p}}m}{N_{\mathrm{F}}}}\left|x_{k,i}(m)\right|^2 \tag{A·4}$$

Therefore, the correlation matrix

$$\begin{aligned} \mathbf{R}_{\mathrm{x}}(m) &= \begin{pmatrix} r_m(1,1) & \cdots & r_m(1,N_{\mathrm{d}}) \\ \vdots & \ddots & \vdots \\ r_m(N_{\mathrm{d}},1) & \cdots & r_m(N_{\mathrm{d}},N_{\mathrm{d}}) \end{pmatrix} \\ &\approx \sum_{i=1}^{K}\left|x_{k,i}(m)\right|^2\begin{pmatrix} 1 & \cdots & \mathrm{e}^{\mathrm{j}2\pi\frac{a_i(N_{\mathrm{d}}-1)N_{\mathrm{p}}m}{N_{\mathrm{F}}}} \\ \vdots & \ddots & \vdots \\ \mathrm{e}^{-\mathrm{j}2\pi\frac{a_i(N_{\mathrm{d}}-1)N_{\mathrm{p}}m}{N_{\mathrm{F}}}} & \cdots & 1 \end{pmatrix} \end{aligned} \tag{A·5}$$

If the number of the vectors N_{R} becomes infinity, the correlation matrix $\mathbf{R}_{\mathrm{x}}(m)$ will become exactly the term in the right hand side of (A·5).

Satoshi Denno received the M.E. and Ph.D. degrees from Kyoto University, Kyoto, Japan in 1988 and 2000, respectively. He joined NTT radio communications systems labs, Yokosuka, Japan, in 1988. He was seconded to ATR adaptive communications research laboratories, Kyoto, Japan in 1997. From 2000 to 2002, he worked for NTT DOCOMO, Yokosuka, Japan. In 2002, he moved to DOCOMO communications laboratories Europe GmbH, Germany. From 2004 to 2011, he worked as an associate professor at Kyoto University. Since 2011, he is a full professor at graduate school of natural science and technology, Okayama University. From the beginning of his research career, he has been engaged in the research and development of digital mobile radio communications. In particular, he has considerable interests in channel equalization, array signal processing, Space time codes, spatial multiplexing, and multimode reception. He won the Best paper award of the 19th international symposium on wireless personal multimedia communications (WPMC2016), and the outstanding paper award of the 23rd international conference on advanced communications technology (ICAT2021). He received the excellent paper award and the best paper award from the IEICE in 1995 and from the IEICE communication society in 2020, respectively.

Yafei Hou received his Ph.D. degrees from Fudan University, China and Kochi University of Technology (KUT), Japan in 2007. He was a post-doctoral research fellow at Ryukoku University, Japan from August 2007 to September 2010. He was a research scientist at Wave Engineering Laboratories, ATR Institute International, Japan from October 2010 to March 2014. He was an Assistant Professor at the Graduate School of Information Science, Nara Institute of Science and Technology, Japan from April 2014 to March 2017. He became an Assistant Professor at the Graduate School of Natural Science and Technology, Okayama University, Japan from April 2017. He is a guest research scientist at Wave Engineering Laboratories, ATR Institute International, Japan from October 2016. His research interest are communication systems, wireless networks, and signal processing. He received IEICE (the Institute of Electronics, Information and Communication Engineers) Communications Society Best Paper Award in 2016 and Best Tutorial Paper Award in 2017. Dr. Hou is a senior member of IEEE and member of IEICE.